NEW APPROACHES IN B_1-MAPPING COMPENSATION FOR *IN VIVO* QUANTITATIVE ^{19}F MR MOLECULAR IMAGING USING UTE BSSFP

Matthew J Goette[1], Todd A Williams[1], John S Allen[1], Jochen Keupp[2], Gregory M Lanza[1], Samuel A Wickline[1], and Shelton D Caruthers[1]
[1]*C-TRAIN, Washington University in St. Louis, St. Louis, MO, United States,* [2]*Philips Research Europe, Hamburg, Germany*

Target Audience: Basic researchers interested in quantitative molecular imaging, particularly of targeted contrast agents and non-proton agents, as well as imaging scientists studying applications of B_1 mapping.

Purpose: Quantitative MR molecular imaging allows for the detection of targeted contrast agents to diagnose disease states and monitor response to therapy, such as angiogenic therapy in peripheral vascular disease[1] and anti-angiogenic therapy in atherosclerosis and cancer[2] with $\alpha_v\beta_3$-integrin targeted perfluorocarbon (PFC) nanoparticles. Recently, ^{19}F MR using a ^{19}F/^{1}H dual-tuned RF coil has been utilized to directly image and quantify the fluorinated core of these PFC nanoparticle (NP) emulsions[3]. Ultra-short echo time (UTE) balanced steady state free precession (bSSFP) sequences have been shown to be much more sensitive to ^{19}F imaging agents than other techniques[4]. However, low concentrations of these fluorine agents in the body, even in the absence of any physiological background signal, in conjunction with varying RF coil sensitivity profiles (i.e. B_1-field inhomogeneities) raises obstacles to optimized imaging and accurate quantification[5]. This study presents a strategy to more accurately quantify the sparse ^{19}F signal from PFC NP emulsions with a ^{1}H image-based Actual Flip Angle (AFI)[6] B_1-mapping correction to the ^{19}F and ^{1}H images.

Methods: In accordance with institution-approved protocols, New Zealand White Rabbits (2 kg) were implanted with a VX2 adenocarcinoma tumor (2-3 cm) in the hind leg[7]. Angiogenesis imaging was performed 2 weeks post implantation (tumor size ~ 15 mm), under ketamine/xylazine anesthesia. An $\alpha_v\beta_3$-integrin targeted perfluoro-15-crown-5-ether (PFCE: $C_{10}F_{20}O_5$) nanoparticle emulsion (20 vol%) was prepared as previously published[8], and injected intravenously 3 hours before imaging. MR data were acquired on a 3.0 T clinical whole-body scanner (Achieva, Philips Healthcare, Best, The Netherlands) with a dual ^{19}F/^{1}H spectrometer system and a dual-tuned transmit/receive single loop surface RF coil (7×12 cm). A simultaneous ^{19}F/^{1}H 3D UTE bSSFP imaging sequence with Wong-type 3D radial readout trajectory[9] was used with: 140 mm FOV, matrix 64^3, isotropic voxel Δx = 2.3 mm, exBW = 4 kHz centered on PFCE peak, pBW = 400 Hz, α = 30°, TR/TE = 2.32/0.13 ms, Nyquist radius = 0.23, NSA = 56, 35 min scan time. The B_1 field was mapped using an Actual Flip-angle Imaging (AFI) sequence with: 140 mm FOV, 96^2 matrix, 15 4-mm slices, 1.4×1.4×0.6 mm resolution, α = 70°, 2.8 min scan time. Using the flip angle map [AFI = $\alpha_{requested}/\alpha_{nominal}$] and a model of the SPGR signal [Eq. 1], a spatially-dependent calibration mask (ρ) was calculated [Eq. 2] in MATLAB (MathWorks, Inc., Natick, MA) and used to compensate the ^{1}H and ^{19}F signal intensities of the SPGR molecular imaging sequence by dividing each image by ρ, pixel by pixel. Importantly, the same correction scheme was performed on the imaging slice that contained the fluorine standard (150 mM_{19F}) to which the bound nanoparticle ^{19}F signal was compared for quantitation.

$$bSSFP = k\sin\alpha\sqrt{E_2}\,\frac{1-E_1}{1-E_1E_2-(E_1-E_2)\cos\alpha} \quad \text{[Eq. 1]} \; ; \quad \rho = AFI*\sin(AFI*\alpha_{nom})\,\frac{1-E_1}{1-E_1E_2-(E_1-E_2)\cos(AFI*\alpha_{nom})} \quad \text{[Eq.2]} \; ; \quad E_1 = e^{-TR/T_1} \; ; \quad E_2 = e^{-TE/T_2}$$

Results and Discussion: PFC NP targeted the tumor neovasculature, providing localized ^{19}F signal as expected. Figure 1 displays the uncorrected (a) and corrected (d) ^{1}H images with the ^{19}F signal superimposed, using the AFI B_1 map (b) and Eq. 2 to calculate a calibration mask (c). After correction, the ^{1}H signal intensity profile as a function of distance from the surface coil (located at right) is improved. After the same correction to the ^{19}F signal, the measured concentration of nanoparticles when compared to a standard was 25.5 ± 2.5 mM_{19F}, versus 20.0 ± 2.3 mM_{19F} before correction. This *in vivo* application of B_1 correction for UTE bSSFP acquired ^{19}F/^{1}H data displays the applicability of such a technique in the preclinical setting, which corroborates with phantom and *in vitro* results. While these data were acquired with, and benefits from, dual-tuned RF coils, this technique of using ^{1}H AFI data to correct ^{19}F molecular imaging data would work with multiple single-tuned coils if the B_1 fields for the two nuclei are the same.

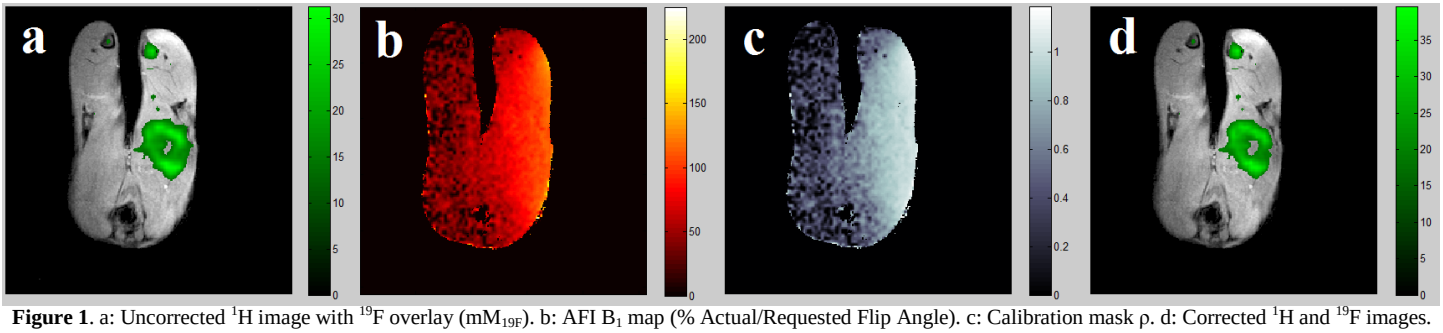

Figure 1. a: Uncorrected ^{1}H image with ^{19}F overlay (mM_{19F}). b: AFI B_1 map (% Actual/Requested Flip Angle). c: Calibration mask ρ. d: Corrected ^{1}H and ^{19}F images.

Conclusion: An image-based B_1-mapping correction can be used to correct signal intensities for simultaneously acquired ^{1}H and ^{19}F images of angiogenesis in an *in vivo* rabbit model. This technique results in a more homogeneous ^{1}H image of the anatomy and facilitates measurement of bound $\alpha_v\beta_3$-integrin targeted nanoparticles with ^{19}F imaging, correcting for known B_1 inhomogeneities. Correction techniques such as this one are required to improve accuracy and repeatability of measurements of molecular imaging agents in preclinical and clinical trials, thereby facilitating translation of molecular imaging, and in particular ^{19}F imaging using fluorinated nanoparticles, into the clinic.

References

1. Winter, et al. Magn Reson Med. 2010;**64**:369-376.
2. Lanza, et al. Eur J Nucl Med Mol Img. 2010;**37**: S114-S126.
3. Caruthers, et al. MedicaMundi. 2010;**54**(2): 5-13 (2010).
4. Keupp, et al. Proc Intl Soc Mag Reson Med 18. 2010.
4. Keupp, et al. Proc Intl Soc Mag Reson Med 15. 2007.
5. Yarnykh. Magn Reson Med. 2007;**57**(1):192-200.
6. Hu, et al. Int J Cancer. 2007;**120**(9):1951-1957.
7. Keupp, et al. Mag Reson Med. 2011;**66**(4): 1116-1122.
8. Wong, et al. Mag Reson Med. 1994; 32:778.